

Role of positional disorder in fully textured ensembles of Ising-like dipoles

Juan J. Alonso ^{1,*}, B. Allés ^{2,†}, J. G. Malherbe ^{3,‡} and V. Russier ^{3,§}

¹*Física Aplicada I and Instituto Carlos I de Física Teórica y Computacional, Universidad de Málaga, 29071 Málaga, Spain*

²*INFN, Sezione di Pisa, Largo Pontecorvo 3, 56127 Pisa, Italy*

³*ICMPE, UMR 7182, CNRS and UPE, 2-8 rue Henri Dunant, 94320 Thiais, France*



(Received 20 July 2023; revised 8 September 2023; accepted 19 September 2023; published 4 October 2023)

We study by numerical simulation the magnetic order in ensembles of randomly packed magnetic spherical particles which, induced by their uniaxial anisotropy in the strong coupling limit, behave as Ising dipoles. We explore the role of the frozen disorder in the positions of the particles assuming a common fixed direction for the easy axes of all spheres. We look at two types of spatially disordered configurations. In the first one we consider isotropic positional distributions which can be obtained from the liquid state of the hard sphere fluid. We derive the phase diagram in the T - Φ plane, where T is the temperature and Φ is the volume fraction. This diagram exhibits long-range ferromagnetic order at low T for volume fractions above the threshold $\Phi_c = 0.157$ predicted by mean-field calculations. For $\Phi \lesssim \Phi_c$ a spin-glass phase forms with the same marginal behavior found for other strongly disordered dipolar systems. The second type of spatial configurations we study are anisotropic distributions that can be obtained by freezing a dipolar hard sphere liquid in its polarized state at low temperature. This structural anisotropy enhances the ferromagnetic order present in isotropic hard sphere configurations.

DOI: [10.1103/PhysRevB.108.134404](https://doi.org/10.1103/PhysRevB.108.134404)

I. INTRODUCTION

Advances in nanotechnology have permitted us to synthesize nanoparticles (NPs) of various sizes and shapes, with or without nonmagnetic coating layers, and to create monodisperse systems of NPs with a certain control on their spatial distribution [1]. Small enough NPs (with diameters of about 10–30 nm) have a single domain that behaves like a magnetic dipole [2].

Furthermore, the internal structure of the NP gives rise to the magnetocrystalline anisotropy energy (MAE) tending to orient the dipoles along local easy axes. Under such a circumstance magnetic spin flips have a nonvanishing energetic cost E_a [3,4]. For sufficiently dense packings, the interaction energy E_{dd} between nearby dipoles can be comparable to E_a . For example, for compact packings of bare maghemite nanoparticles the ratio E_a/E_{dd} is approximately [5] $E_a/E_{dd} \approx 6$. For such systems E_{dd} can induce complex collective behavior endowing them with a rich phenomenology, mainly at low temperature [4,6,7]. Indeed, the spatial variations of the dipolar fields lead to geometric frustration, making these systems rather sensitive to the relative positions and directions of their dipoles. For example, dipoles placed in well-ordered crystalline arrangements exhibit ferromagnetic (FM) or anti-ferromagnetic order depending on the lattice geometry [8].

In the strong MAE limit the dipole of each NP points up or down nearly parallel to its local easy axis, leading to a dipolar Ising-like model [9] in which only E_{dd} play a central role.

The study of magnetic order in systems of magnetic NPs is an active field of research [10,11]. Its interest ranges from fundamental physics because of the need to understand the collective effects of samples of NPs to their applications in a broad class of technological problems like data storage [12] and nanomedicine [13].

When the arrangements of NPs are obtained by freezing the carrier fluid in colloidal suspensions of NPs [14] or by compacting powders of granular solids [15], disorder both in dipole orientations and in position results. This double disorder along with the geometric frustration inherent in dipolar interactions may give rise to dipolar spin-glass behavior. This has been observed experimentally in frozen ferrofluids [14,16] and in pressed powders of NPs [6,15].

The role played by the orientational disorder (called texturation) has been studied using Monte Carlo simulations in crystalline lattices [17] and in random distributions [18]. In both cases the magnetic order at low temperature changed from FM to spin-glass (SG) as the orientational disorder increased from textured (parallel axis dipoles) to nontextured (random axis dipoles). The same has been found in nontextured systems by using the ratio E_a/E_{dd} as the disorder parameter [19].

On the other hand, the role played by the disorder in positions in systems of NPs is not completely understood. Heisenberg dipoles with no local anisotropies placed in random dense packings (RDPs) have been studied using Monte Carlo simulations. Given that the dipoles can rotate freely, the frozen disorder is only in positions and depends on the fraction Φ of volume occupied by the NPs. Numerical simulations find FM order for $\Phi \gtrsim 0.49$ and SG order otherwise [20]. In the mean-field approach, Zhang and Widom found FM order for $\Phi \geq 0.295$ under the crude approximation of $g(r) = 1$, where $g(r)$ is the radial distribution function [21].

*jjalonso1@gmail.com

†alles@pi.infn.it

‡malherbe@u-pec.fr

§vincent.russier@cnrs.fr

This discrepancy seems to be due to the spatial correlations at short distances for RDPs.

Reverting to systems of NPs, it must be noticed that the local anisotropy in single-domain NPs is always nonzero. For this reason, the only way to suppress orientational disorder in such systems in order to explore only positional disorder effects is to consider textured systems. It was recently found that the alignment of the easy axes reduces the dipolar field acting on each NP for volume fractions of $0.3 \lesssim \Phi$ [22]. A certain texturation arises naturally in colloidal liquids even in the absence of an external field. Even for moderate values of the volume fraction ($0.25 \lesssim \Phi \lesssim 0.5$), the dipolar hard sphere (DHS) fluid polarizes for temperatures below the ferromagnetic transition temperature, exhibiting anisotropic short-range spatial correlations [23–25].

In this paper we investigate the magnetic order of systems of textured dipoles as a function of the positional disorder in RDPs. For this purpose we will use Ising dipoles that point up and down along a common direction such that the structural disorder comes only from the spatial distribution. For large volume fractions [18,26] previous numerical simulations showed FM order. Instead, for dipolar crystals with strong dilution SG order was observed [27]. We wish to clarify how the degree of spatial disorder in RDPs replaces FM order with SG order.

We study two types of spatially disordered systems of NPs. First, we consider frozen distributions taken from the liquid state of the hard sphere fluid, whose degree of disorder is parametrized by Φ . Our aim is to obtain the phase diagram in the T - Φ plane and investigate the nature of the low-temperature phases. The second type of spatially disordered systems studied in this paper are the distributions that arise from freezing the DHS fluid. They are obtained by cooling to a temperature T_f a fluid of the DHS with a moderate volume fraction Φ below its ferromagnetic transition temperature, which will be denoted by $T_c(\text{DHS}, \Phi)$. Apart from orientational order and spatial disorder, these spatial distributions show a structural anisotropy that increases when T_f diminishes [25]. We wish to discover whether such anisotropic configurations favor FM order in textured systems.

Given that we are interested in equilibrium properties, we assume that the dynamics allow Ising dipoles to flip the orientation in order to reach equilibrium. This is tantamount to choosing a vanishing blocking temperature [3,4]. It is worthwhile to mention that in systems with uniaxial finite anisotropy Monte Carlo simulations indicate the existence of an effective behavior similar to that of Ising dipoles for $E_a/E_{dd} \gtrsim 30$ [19].

This paper is organized as follows. In Sec. II we present the model and details of the Monte Carlo algorithm and introduce the observables that will be measured. We present and discuss our results in Sec. III. A summary and some concluding remarks are given in Sec. IV.

II. MODEL, METHOD, AND OBSERVABLES

A. Model

We study systems of N identical NPs whose dipoles stay oriented along a common fixed direction \hat{a} . They are labeled

with an index $i = 1, \dots, N$. Each NP can be viewed as a sphere of diameter d . Its magnetic moment will be denoted by $\vec{\mu}_i = \mu s_i \hat{a}$, where $s_i = \pm 1$ and μ takes the same value for all spheres. For $s_i = +1$ (-1) the dipole points parallel (antiparallel) to \hat{a} .

The N spheres are placed in frozen disordered configurations in a cube of edge L . The volume fraction occupied by the spheres is $\Phi = N\pi/6(d^3/L^3)$. We assume periodic boundary conditions. The position of each particle remains fixed during the simulations, and only the signs s_i evolve in time, assuming that the dipoles are able to flip up and down along \hat{a} .

The Hamiltonian of the system reads

$$\mathcal{H} = \sum_{i \neq j} \varepsilon_d \left(\frac{d}{r_{ij}} \right)^3 \left(1 - \frac{3(\hat{a} \cdot \vec{r}_{ij})(\hat{a} \cdot \vec{r}_{ij})}{r_{ij}^2} \right) s_i s_j, \quad (1)$$

where $\varepsilon_d = \mu_0 \mu^2 / (4\pi d^3)$ is an energy and μ_0 is the magnetic permeability in vacuum. \vec{r}_{ij} is the position of dipole j as viewed from dipole i , and $r_{ij} = \|\vec{r}_{ij}\|$. Temperatures will be given in units of ε_d/k_B , where k_B is the Boltzmann constant.

We use the word ‘‘configuration’’ to denote a particular realization of positional disorder. Mathematically, it is given by the set of vectors \vec{r}_{ij} , with $i, j = 1, \dots, N$, $i \neq j$, and the nonoverlapping constraint $r_{ij} > d$ to be plugged in (1).

We investigate systems of dipoles for two types of configurations. On the one hand, we choose configurations of hard spheres corresponding to their stable liquid state with given volume fraction Φ . We consider values of Φ ranging from diluted systems with $\Phi = 0.1$ up to the freezing point ($\Phi = 0.49$). These configurations are obtained by using the Lubachevsky-Stillinger algorithm [28–30], in which the spheres, which are initially very small, are allowed to move and collide while growing in size until they reach the desired value of Φ . Their spatial correlations, due to steric effects, are isotropic, being described by the radial distribution function $g(r)$. The amount of disorder of such configurations is a function of Φ .

The second type of configuration appears by freezing colloidal suspensions of NPs. In practice they are obtained from equilibrium states of the DHS fluid model for low T_f in such a way that the states correspond to the phase where the system is polarized without crystalline order [23,24]. These configurations exhibit a large degree of spatial anisotropy which is larger for lower T_f [25]. The degree of disorder of such configurations is a function of Φ and T_f . We have chosen two volume fractions, $\Phi = 0.262$ and $\Phi = 0.45$, with values of the temperature T_f adequate to keep the configurations homogeneous.

Following the usual notation in discussions on SG order, we shall call ‘‘sample’’ any system of NPs after they are placed in a specific distribution of fixed positions, that is, in a specific configuration. Physical results follow by averaging over N_s independent samples. These averages are crucial in systems with strong frozen disorder, for which SG order is expected and where sample-to-sample fluctuations are large. We used about $N_s = 1000$ samples when FM order was present and at least $N_s = 4000$ samples when SG order was present. For the simulations reported in Sec. III B we averaged over $N_s = 1000$ samples for $\beta_f = 0$ and over 250 for $\beta_f > 0$.

B. Method

The systems considered here are expected to enter a SG phase in the case of strong frozen disorder at low T . As is well known, SG phases are difficult to simulate due to the presence of energy landscapes which are beset with barriers and valleys. In order to overcome that difficulty, we used the tempered Monte Carlo algorithm [31], which is specially adapted to facilitate samples wandering through such rough landscapes in an efficient way. More specifically, for each sample we run in parallel n identical replicas at n different temperatures T_i , $i = 1, \dots, n$. After applying 10 Metropolis sweeps [32] to each replica, we exchange neighboring pairs of replicas according to detailed balance. In order to reach equilibrium within a reasonable amount of computer time, we found it useful to choose the highest temperature T_n to be $T_n \gtrsim 2T_c$ and the lowest one T_1 to be $T_1 \gtrsim 0.5T_c$, where T_c is the expected transition temperature from the PM to the ordered phase. We used an arithmetic distribution of temperatures

$$T_i = T_1 + (i - 1)\Delta T, \quad (2)$$

with $\Delta T = 0.05$ and $n \approx 60$ replicas. When necessary, we added some additional temperatures with spacing $\Delta T = 0.025$ for the low-temperature region $0.5T_c \lesssim T \lesssim 1.1T_c$. Only for the systems which are harder to equilibrate (this occurs with $N = 1728$ and $\Phi \leq 0.18$) do we use the inverse linear distribution [33]

$$\frac{1}{T_i} = \frac{1}{T_1} + \left(\frac{1}{T_n} - \frac{1}{T_1} \right) \frac{i - 1}{n - 1} \quad (3)$$

by choosing $n = 70$ and $T_1 \approx 0.8T_c$. The thermal equilibration times t_0 are estimated following the procedure described in Ref. [34]. For the above list of temperatures we used $t_0 = 10^6$ Metropolis sweeps for equilibration and took thermal averages for each given sample within the interval $[t_0, 2t_0]$. A second average over N_s samples is needed to obtain physical results. For an observable u , this double average will be denoted by $\langle u \rangle$.

The lattice volumes were cubes of edge L with periodic conditions at the boundaries. The long-range nature of the dipolar-dipolar interaction is treated using Ewald's sums [35]. Details on the use of Ewald's sums for dipolar systems are given in Ref. [36]. We chose $\alpha = 4/L$ as the splitting parameter and computed the sum in real space with a cutoff $r_c = L/2$ and the sum in the reciprocal space with a cutoff $k_c = 10$ [36]. Given that in the case of weak frozen disorder the systems are expected to show FM order, we performed the Ewald sums using the so-called conducting external conditions, with surrounding permeability $\mu' = \infty$. This technique allows us to avoid shape-dependent depolarizing effects [23,37].

C. Observables

The main goal of this work has been the determination of the magnetic order as a function of the degree of disorder in the positions of the particles. On general grounds it is expected that any increase in disorder leads to a reduction of the area occupied by FM order in the phase diagram and an equivalent increase of the area corresponding to SG order. To characterize both types of magnetic order we employed

several observables. The first is the specific heat

$$c \equiv \frac{1}{NT^2} [\langle \mathcal{H}^2 \rangle - \langle \mathcal{H} \rangle^2], \quad (4)$$

obtained from fluctuations of energy, where the energy is

$$e \equiv \langle \mathcal{H} \rangle / N. \quad (5)$$

Also, to distinguish FM order, we used the spontaneous magnetization

$$m \equiv \frac{1}{N} \sum_i s_i \quad (6)$$

and evaluated its momenta $m_p \equiv \langle |m|^p \rangle$ for $p = 1, 2, 4$ and, from them, the magnetic susceptibility

$$\chi_m \equiv \frac{N}{k_B T} (m_2 - m_1^2) \quad (7)$$

and the Binder cumulant

$$B_m \equiv \frac{1}{2} \left(3 - \frac{m_4}{m_2^2} \right), \quad (8)$$

which permits us to extract the transition temperature between the FM and paramagnetic (PM) phases.

To mark the onset of the SG phase, we evaluated the Edwards-Anderson overlap parameter [38], defined as

$$q \equiv \frac{1}{N} \sum_i s_i^{(1)} s_i^{(2)}, \quad (9)$$

for any given sample, where $s_i^{(1)}$ and $s_i^{(2)}$ are the signs of s_i at site i of two replicas labeled (1) and (2) for that sample. Each replica is allowed to evolve independently at the same temperature. Like for m , we also measured the momenta $q_p \equiv \langle |q|^p \rangle$ for $p = 1, 2, 4$ and, from them, the Binder cumulant

$$B_q \equiv \frac{1}{2} \left(3 - \frac{q_4}{q_2^2} \right). \quad (10)$$

To identify the transition temperature between the PM and SG phases we employed the so-called SG correlation length ξ_L , which is given by

$$\xi_L^2 \equiv \frac{1}{4 \sin^2(k/2)} \left(\frac{\langle q^2 \rangle}{\langle |q(\vec{k})|^2 \rangle} - 1 \right), \quad (11)$$

where $q(\vec{k})$ is

$$q(\vec{k}) \equiv \frac{1}{N} \sum_j s_j^{(1)} s_j^{(2)} e^{i\vec{k} \cdot \vec{r}_j}, \quad (12)$$

with \vec{r}_j being the position of the j th NP, $\vec{k} = (2\pi/L, 0, 0)$ and $k = \|\vec{k}\| = 2\pi/L$ [39].

Errors in the measurements of these quantities were calculated as the mean-square deviations of the sample-to-sample fluctuations.

III. RESULTS

A. Phase diagram for isotropic HS-like configurations

In this section we investigate the magnetic order as a function of the volume fraction Φ for frozen configurations

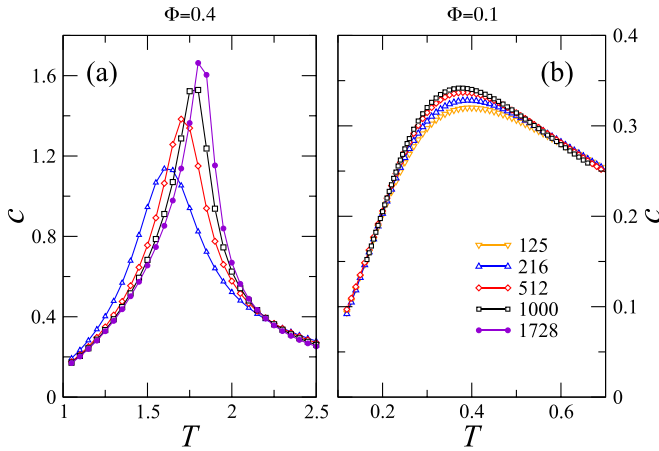


FIG. 1. (a) Plots of the specific heat c versus T for volume fraction $\Phi = 0.4$. Symbols ∇ , \triangle , \diamond , \square , and \bullet stand for $N = 125, 216, 512, 1000$, and 1728 , respectively. (b) Same as in (a), but for volume fraction $\Phi = 0.1$.

obtained from equilibrium states of hard sphere fluids in the range $0 < \Phi \lesssim 0.49$. Φ measures the degree of spatial disorder on such configurations. We will show that for decreasing Φ (which means increasing disorder) SG order replaces the FM order.

A first overview can be grasped from Figs. 1 and 2. Figure 1(a) displays plots of the specific heat c vs T for $\Phi = 0.4$. The curves exhibit a marked lambda-shaped peak. Their evident dependence on the number of NPs indicates the presence of a singular point in the curve that corresponds to $N \rightarrow \infty$ at $T_c \approx 1.9$. That singular behavior is expected in PM-FM second-order transitions. Data are consistent with a logarithmic divergence of c with N . Figure 1(b) shows the plots obtained for $\Phi = 0.1$. In contrast to the previous ones, these plots are smooth and depend little on the sample size. So there is no sign of any singular behavior. This is expected in PM-SG transitions with strong structural disorder.

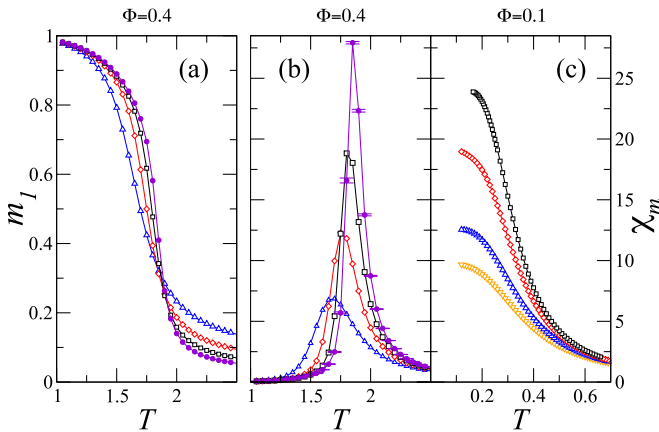


FIG. 2. (a) Plots of the magnetization m_1 versus T for volume fraction $\Phi = 0.4$. Symbols ∇ , \triangle , \diamond , \square , and \bullet stand for $N = 125, 216, 512, 1000$, and 1728 , respectively. (b) Plots of the magnetic susceptibility χ_m versus T for volume fraction $\Phi = 0.4$. Symbols are the same as in (a). (c) Same as (b), but for volume fraction $\Phi = 0.1$.

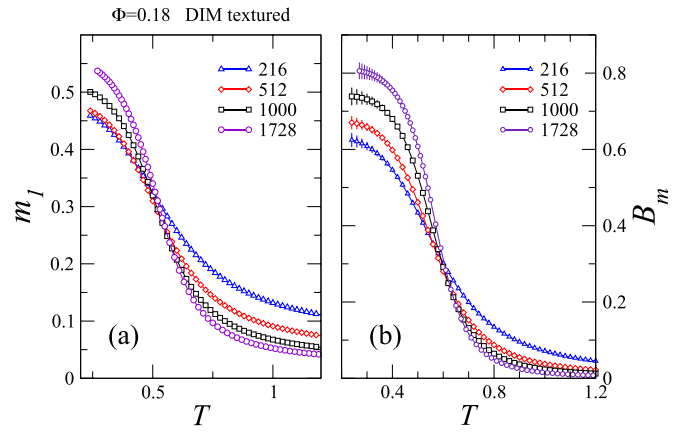


FIG. 3. (a) Plots of the magnetization m_1 vs T for $\Phi = 0.18$. Symbols \triangle , \diamond , \square , and \circ stand for $N = 216, 512, 1000$, and 1728 , respectively. (b) Plots of the Binder cumulant of the magnetization B_m vs T for $\Phi = 0.18$. Symbols are the same as in (a).

FM order entails the presence of nonvanishing magnetization m . Figure 2(a) displays m_1 vs T for $\Phi = 0.4$ at several N . It shows that m_1 tends to nonzero values for $N \rightarrow \infty$ and low T , revealing the existence of strong FM order. The curves plotted in Fig. 2(b) for the magnetic susceptibility χ_m vs T confirm this conclusion because they show peaks that become sharper for large N . An extrapolation of the positions of the maxima of those peaks vs $1/N$ provides a value for the transition temperature, $T_c(\Phi = 0.4) \simeq 1.9(1)$, in agreement with the estimated T_c obtained from the analysis of Fig. 1(a). For $T < T_c$ we find that χ_m does not diverge with N , a fact that validates the above conclusions on FM order. All that is in contrast to the results obtained for $\Phi = 0.1$, shown in Fig. 2(c), where we see how the values of χ_m increase with N for low T . Data are consistent with the trend $\chi_m \sim N^p$ for $p \approx 0.45$ and $T \lesssim 0.2$. This behavior suggests the existence of a SG phase.

Let us discuss now the threshold value of Φ at which the FM order disappears. Mean-field calculations predict that FM order persists for $\Phi \geq \Phi_c = \pi/20 \sim 0.157$ [21].

The plots in Fig. 3 show that the FM order persists at $\Phi = 0.18$. The curves of m_1 vs T in Fig. 3(a) indicate an increase in magnetization with N at low T , although they also exhibit relevant finite-size effects. The Binder parameter in Fig. 3(b) allows us to determine the transition temperature within good precision. In general this parameter tends to 1 for $N \rightarrow \infty$ in FM phases, while from the law of large numbers it follows that in PM phases $B_m \rightarrow 0$ as N increases. On the other hand, since B_m is dimensionless, it must be independent of N at the critical point. As a consequence, curves of B_m vs T for different values of N cross at T_c for second-order transitions. Instead, in the presence of an intermediate marginal phase of quasi-long-range FM order, the curves do not cross but join. Plots of B_m vs T for several N are shown in Fig. 3(b) for $\Phi = 0.18$. Those curves cross at a well-defined critical temperature for $N \geq 512$ [40]. With similar results obtained for $\Phi \geq 0.17$, we can draw a line of transition between PM and FM phases.

The corresponding plots for $\Phi = 0.14$ are shown in Fig. 4. The qualitatively different results illustrate the absence of FM

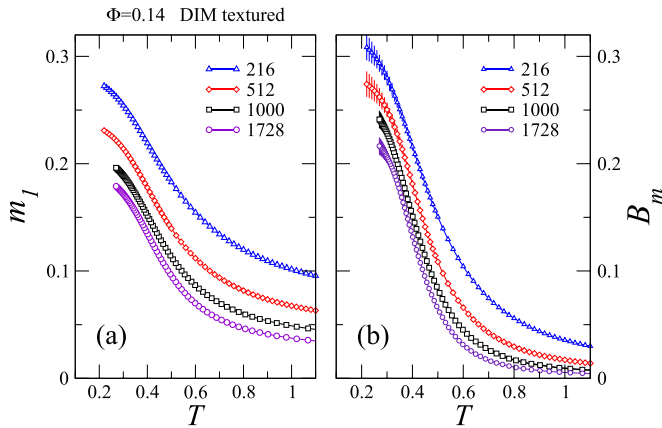


FIG. 4. (a) Plots of the magnetization m_1 vs T for $\Phi = 0.14$. Symbols Δ , \diamond , \square , and \circ stand for $N = 216, 512, 1000$, and 1728 , respectively. (b) Plots of the Binder cumulant of the magnetization B_m vs T for $\Phi = 0.18$. Symbols are the same as in (a).

order at this value of Φ . The plots of the magnetization in Fig. 4(a) show that m_1 gradually decreases as N increases for all T . The data for m_1 at low temperature agree with the algebraic decay $m_1 \sim N^p$ for $p < 1/2$; hence, a marginal order is *a priori* not excluded. However, the plots of B_m vs T from Fig. 4(b) show clearly that B_m vanishes for $N \rightarrow \infty$ for all T , and this means that the FM order is short range even at low temperature. We obtained similar plots for all analyzed values of Φ in the range $\Phi \leq 0.15$, and this fact excludes FM order.

It is then imperative to investigate whether at those values of Φ the FM phase is replaced by SG order. For this purpose we evaluate the overlap parameter q_1 in Fig. 5. In Fig. 5(a) we show plots of q_1 vs T for $\Phi = 0.14$. It is instructive to compare these plots with those for m_1 in Fig. 4(a) for the

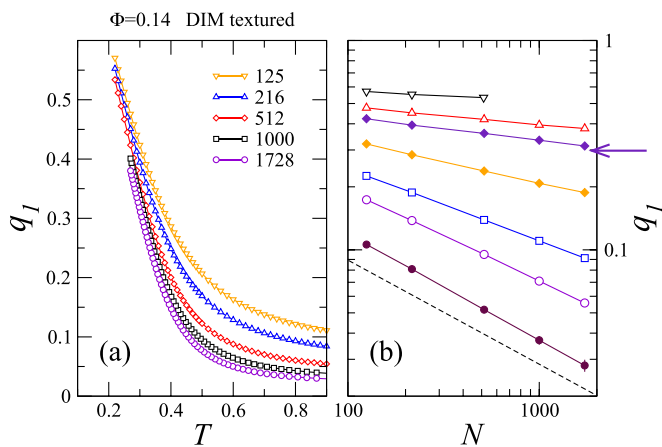


FIG. 5. (a) Plots of the SG overlap parameter q_1 vs T for $\Phi = 0.14$. Symbols ∇ , Δ , \diamond , \square , and \circ stand for $N = 125, 216, 512, 1000$, and 1728 , respectively. (b) Log-log plots of q_1 vs N for several temperatures at $\Phi = 0.14$. From top to bottom, ∇ , Δ , \diamond , \square , \circ , and \bullet stand for $T = 0.22, 0.27, 0.31, 0.37, 0.47, 0.57$, and 0.96 , respectively. The arrow marks the data set corresponding to the SG-PM transition temperature. The dashed line shows the $N^{-1/2}$ decay expected for a paramagnet.

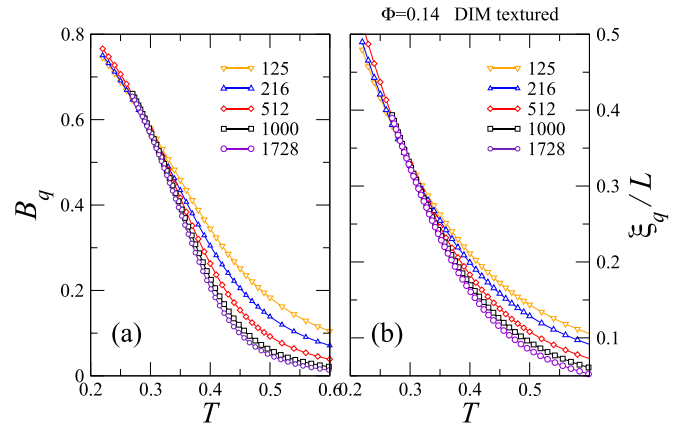


FIG. 6. (a) Plots of the SG correlation length ξ_L/L vs T for $\Phi = 0.14$. Symbols ∇ , Δ , \diamond , \square , and \circ stand for $N = 125, 216, 512, 1000$, and 1728 , respectively. (b) Plots of the SG correlation length Ξ_L/L vs T for $\Phi = 0.14$. Symbols are the same as in (a).

same value of Φ . We notice that like for m_1 , the overlap q_1 decreases when N increases for all temperatures. To determine whether q_1 tends to zero in the limit $N \rightarrow \infty$, we show log-log plots of q_1 vs N in Fig. 5(b). Data in these plots are consistent with the behavior $q_1 \sim 1/N^p$ at low temperatures, where p is a T -dependent exponent. Thus, for example, at $T = 0.31$ we obtain $p \simeq 0.11$. The expected behavior for a PM phase is $N^{-1/2}$, but we found it only at high temperature. These properties could be due to the presence of SG with quasi-long-range order at low T . To verify that we examine the behaviors of B_q and ξ_L/L in terms of T . Recall that, indeed, in the thermodynamic limit $B_q \rightarrow 1$ when there is strong SG order, becomes zero in the PM phase, and tends to an intermediate value at critical points. A similar trend is expected for dimensionless magnitudes like ξ_L/L with a caveat: in the case of strong order, this quantity diverges as $N^{1/2}$ instead of going to 1. This makes the splaying out of curves for ξ_L/L for different sizes at low temperatures more prominent than for B_q , and the crossing points are clearer for second-order transitions [39].

The curves B_q vs T for $\Phi = 0.14$ shown in Fig. 6(a) merge at T below a certain value $T_{sg} \simeq 0.31(2)$, rather than crossing. The spread that those curves exhibit for $T < T_{sg}$ becomes almost zero for $N \geq 512$. Thus, B_q does not tend to 1 in the thermodynamic limit. Then, the curves B_q collapse for $N \rightarrow \infty$ and $T \leq T_{sg}$, which is consistent with the algebraic decay found for q_1 . The plots of ξ_L/L vs T in Fig. 6(b) exhibit a similar behavior. All that emphasizes that SG order with quasi-long-range order exists, which happens in other systems with NPs and strong structural disorder.

The temperature T_{sg} that marks the transition between PM and SG orders is a function of Φ , and for that reason it will be represented as $T_{sg}(\Phi)$. The fact that the merging of different curves is dominant over crossing makes the determination of $T_{sg}(\Phi)$ less precise than for the PM-FM transition. In any case $T_{sg}(\Phi)$ is quite smooth as a function of Φ for strong dilution. For $\Phi = 0.1$ we obtained $T_{sg}/\Phi = 1.9(1)$, in agreement with the relation $T_{sg} = x$ found in the limit of strong dilution for systems of dipoles in crystalline simple cubic (SC) lattices with a fraction x of occupied sites [27]. For a diluted system of

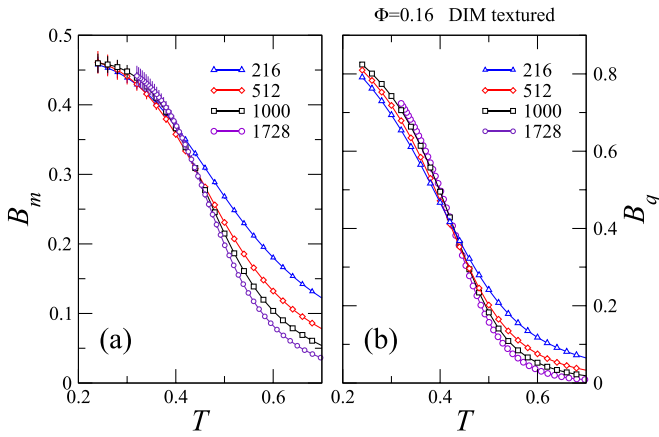


FIG. 7. (a) Plots of the Binder cumulant B_m vs T for $\Phi = 0.16$. Δ , \diamond , \square , and \circ stand for systems with $N = 216, 512, 1000$, and 1728 dipoles, respectively. (b) Plots of the Binder cumulant for the overlap parameter B_q vs T for $\Phi = 0.16$. Symbols are the same as in (a).

spheres with SC order, this relation reads $T_{sg}/\Phi = 1/\Phi_{SC} \simeq 1.91$, where Φ_{SC} is the volume fraction for SC lattices.

As a last step we determine the low-temperature boundary of the FM phase. Mean-field theory predicts the onset of FM order for $T = 0$ at $\Phi_c = 0.157$. Let us examine first the data obtained for $\Phi = 0.16$. Plots of B_q vs T for various sizes are shown in Fig. 7(b). We estimate that the curves cross at $T_c \simeq 0.44$. For $T < T_c$ we find (not shown) that q does not vanish in the thermodynamic limit, a fact that points to the presence of SG order. Contrarily, the curves of B_m vs T shown in Fig. 7(a) merge at low temperatures. In particular, the curves for $N = 1000$ and $N = 1177$ fall on top of each other within the error bars for $T < T_c$. This suggests that the transition line between FM and SG lies at $\Phi \simeq 0.16$ at low temperature.

This line of critical points can be recovered in a more precise way with data obtained from simulations in the range $0.13 < \Phi < 0.18$. To this end, we prepare plots of B_m vs Φ at different N along isotherms for T below the PM region. Figures 8(a) and 8(b) show the plots for the isotherm at $T = 0.28$

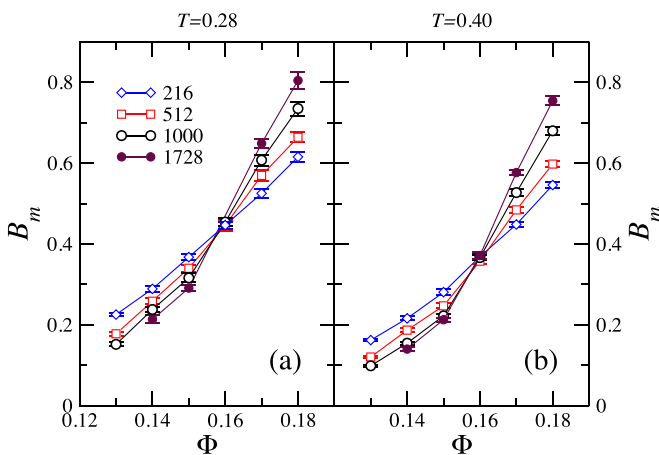


FIG. 8. (a) Plots of the Binder cumulant B_m vs Φ for $T = 0.28$. \diamond , \square , \circ , and \bullet stand for systems with $N = 216, 512, 1000$, and 1728 dipoles respectively. (b) The same as (a), but for temperature $T = 0.40$.

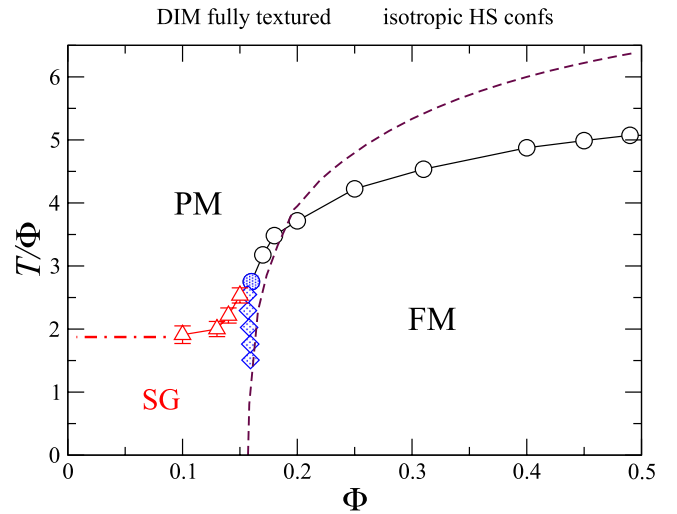


FIG. 9. Phase diagram in the plane (T, Φ) for the fully textured dipolar Ising model in random HS-like configurations. The \circ symbols stand for the PM-FM transition obtained from the B_m vs T plots. The Δ symbols stand for the PM-SG transition obtained from the B_q vs T plots. The \diamond symbols represent the FM-SG transition and follow from the B_m vs Φ plots. Error bars are smaller than the size of these symbols. The dashed line indicates a mean-field calculation by Zhang and Widom [21]. The horizontal red dashed line comes from previous calculations for strongly diluted DIS in crystals.

and $T = 0.4$, respectively. Recall that B_m diminishes as N increases in the SG phase, while in the FM phase B_m increases with N . As shown in both panels, we find that the curves of B_m vs Φ cross at the transition $\Phi_c(T)$. A very precise result can be obtained if we have many values of Φ available. The transition line $\Phi_c(T)$ is almost vertical at $\Phi = 0.160(5)$, in good agreement with mean-field approximation. We also notice the well-defined separation in the curves above and below the crossing point in Fig. 8. This detail rules out the possibility of the presence of critical phases between FM and SG in the region close to $\Phi \simeq \Phi_c(T)$.

The results in this section are gathered in the phase diagram in Fig. 9, which shows the extension of the FM, SG, and PM regions. They are separated by second-order transition lines. The slope of the transition line at low density is nearly zero, so that the ratio T_{sg}/Φ takes a fixed value, $T_{sg}/\Phi \simeq 1.9$. Mean-field theory yields a good approximation of the boundary line of the FM phase at low temperatures [21]. This approximation is carried out by assuming fully random particle positions, which is in contrast to the results obtained for systems of dipoles with no local anisotropy [20], for which the onset found at $\Phi = 0.49$ coincides with the freezing point of the hard sphere fluid. This onset depends on the details of the radial distribution function for short distances [41]. We end this discussion by noting that different from systems of Ising dipoles with orientational disorder [18], we have found for the systems studied in this paper no trace of reentrances or other intermediate phases, which is clearly shown in Fig. 9.

B. FM order on anisotropic DHS fluidlike configurations

In this section we will describe the results obtained by exploring the FM order of textured Ising dipoles placed in

frozen DHS fluidlike distributions of particles. These positional distributions are taken from equilibrium configurations of the DHS fluid at low temperatures T_f [25]. We consider volume fractions in the range $0.25 \lesssim \Phi \lesssim 0.5$, for which the DHS fluid is known to polarize below the transition temperature $T_c(\text{DHS}, \Phi)$ [23,24]. Within this interval of values of Φ and for a wide range of temperatures T_f below $T_c(\text{DHS}, \Phi)$ the equilibrium configurations for the DHS fluid exhibit some partial alignment of the magnetic moments $\hat{\mu}_i$ along a common direction and a certain degree of anisotropy in the positional distribution. At the same time these fluidlike configurations are still homogeneous and show the absence of crystalline order [24]. It is this type of configurations that arises naturally in colloidal suspensions of particles at low temperature.

Any of those equilibrium configurations is determined by the positions \vec{r}_i and the instantaneous orientations of the magnetic moments $\hat{\mu}_i$ of all particles, $i = 1, \dots, N$. At low T_f the orientations exhibit nematic order along a preferred direction \hat{a} . In this case the configurations are said to be *partially textured*.

As is customary when studying nematic order, the direction \hat{a} can be determined as the eigenvector related to the largest eigenvalue of the so-called nematic tensor [37]

$$\bar{Q}_n = \frac{1}{2N} \sum_i (3\hat{\mu}_i \hat{\mu}_i - \bar{I}). \quad (13)$$

Thus, the degree of texturation can be quantified by the value of the nematic order parameter λ_n . Similarly, the degree of anisotropy in the disordered positional distribution can be assessed by the *structural* nematic order parameter λ_s associated with the tensor

$$\bar{Q}_s = \frac{1}{2N_{nm}} \sum_{nm} (3\hat{r}_{nm} \hat{r}_{nm} - \bar{I}), \quad (14)$$

where \hat{r}_{nm} are the normalized relative positions $\hat{r}_{ij} \equiv \vec{r}_{ij}/r_{ij}$ between pairs of particles whose r_{ij} distance is smaller than a threshold value chosen to be $r_s = 1.2d$ and N_{nm} is the number of such pairs [42]. λ_s is the largest eigenvalue of \bar{Q}_s and measures the degree of alignment of the set of \hat{r}_{nm} along a preferred direction.

The behavior of those eigenvalues was explored for $\Phi = 0.45$ and $\Phi = 0.262$ in Ref. [25]. Plots of λ_n and λ_s versus the inverse temperature $\beta_f = 1/T_f$ are given for $\Phi = 0.45$ and $N = 1177$ in the inset of Fig. 10. The plateaus found for $\beta_f \lesssim \beta_c(\text{DHS}, \Phi) = 4$ with $\lambda_s \simeq \lambda_n \simeq 0$ indicate that the configurations remain isotropic for temperatures above the PM-FM transition [the notation $\beta_c(\text{DHS}, \Phi) \equiv 1/T_c(\text{DHS}, \Phi)$ has been used]. In contrast, for $\beta_f \gtrsim 4$ both λ_n and λ_s increase with β_f , indicating that the double anisotropy strengthens as temperature is lowered. For $\Phi = 0.262$, where $\beta_c(\text{DHS}, \Phi) = 7.7$, the behavior is qualitatively the same, apart from the fact that chains of spheres seem to form at very low temperature instead of the homogeneous configurations observed for $\Phi = 0.45$.

Up to now, we have described equilibrium DHS fluidlike configurations at low T which exhibit partial texturation in the orientations of the dipoles as well as structural anisotropy in their positions [25]. However, given that this work is aimed at the study of the role of frozen positional disorder, we proceed

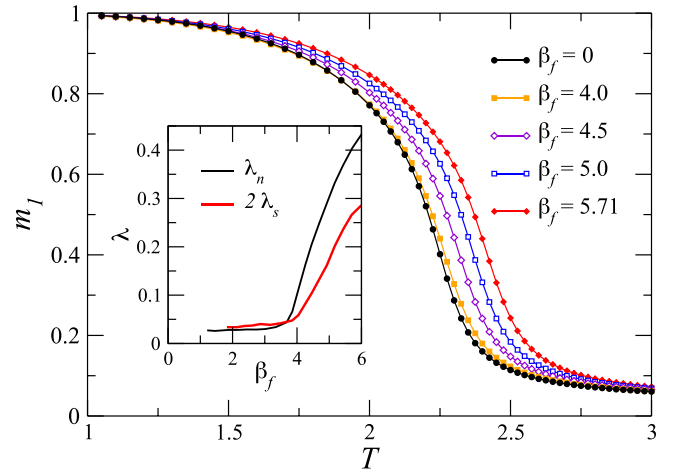


FIG. 10. Plots of the magnetization m_1 vs T for ensembles of $N = 1177$ dipoles placed on anisotropic frozen configurations obtained for $\Phi = 0.45$ and the inverse freezing temperatures β_f indicated in the legend. The inset shows the structural λ_s and orientational λ_n nematic order parameters for the DHS fluid versus the inverse temperature β_f for density $\Phi = 0.45$ and $N = 1177$ (data taken from Ref. [25]).

by studying fully textured systems of DHS fluidlike configurations in equilibrium. Once one of these configurations is picked, i.e., once the sets of positions \vec{r}_i and momenta $\hat{\mu}_i$ are fixed throughout the lattice, the frozen textured distribution is built by first computing the nematic tensor \bar{Q}_n and then choosing the nematic director \hat{a} of \bar{Q}_n as the common direction along which all the Ising dipoles are placed.

The question now is how the remaining structural positional anisotropy in those systems affects the order at low T . We do not expect to find any SG order for the volume fractions considered here ($0.25 \lesssim \Phi \lesssim 0.5$). Note, from the previous section, that for $\Phi \lesssim 0.16$ only FM order is expected at low T even for isotropic configurations. Thus, by studying DHS systems we intend to analyze whether the structural positional anisotropy enhances the FM order already present in isotropic hard sphere (HS) configurations.

Curves of magnetization m_1 vs T are shown in Fig. 10 for $\Phi = 0.45$ and $N = 1177$ for various values of $\beta_f = 1/T_f$. The system at low temperature is in a FM phase even for $\beta_f = 0$ in the absence of anisotropy, in agreement with the previous section. The result for $\beta_f \simeq \beta_c(\text{DHS}, \Phi) \simeq 4$ is practically the same as that for $\beta_f = 0$. Only for $\beta_f > 4$ do we see the curves of magnetization move rightwards as β_f increases, a fact that indicates that the increase in anisotropy favors FM order. The susceptibility χ_m vs T curves shown in Fig. 11 exhibit peaks which are typical for ferromagnets. The positions of those peaks for $\beta_f > 4$ shift to the right as β_f increases, indicating that the PM-FM transition temperature T_c increases with the anisotropy.

A precise determination of T_c can be obtained from the crossing points of the Binder parameter vs T for different sizes, as shown in Fig. 12. The inset shows the transition temperature T_c vs β_f for $\Phi = 0.45$. Figure 12 should be compared with the inset of Fig. 10. We can appreciate that T_c increases with β_f only for $\beta_f > \beta_c(\text{DHS}, \Phi) \simeq 4$ when the structural anisotropy quantified by λ_s increases. It is worth mentioning

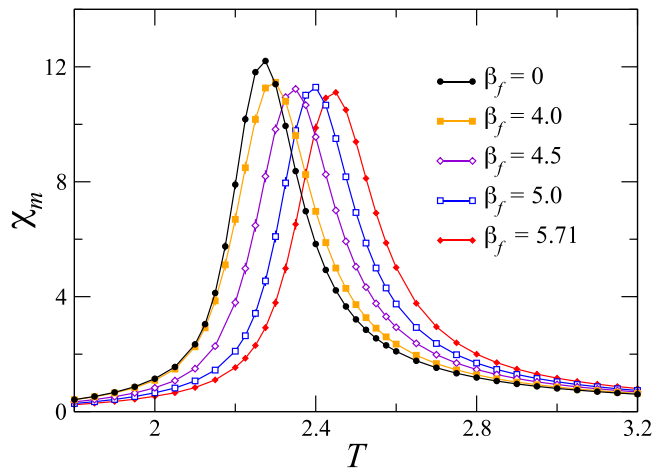


FIG. 11. Plots of the susceptibility χ_m vs T for ensembles of $N = 1177$ dipoles placed on anisotropic frozen configurations obtained for $\Phi = 0.45$ and the inverse freezing temperatures β_f indicated in the legend.

that for $\beta_f \gtrsim 4$ the values of T_c obtained here for fully textured systems along the nematic director \hat{a} practically coincide with the values of T_c found for ensembles of Ising dipoles placed on the same frozen configurations $\{\vec{r}_i\}$ but point up or down along the orientations $\{\hat{\mu}_i\}$ of the original DHS configurations [25]. This suggests that the procedure used in this work for imposing a common direction \hat{a} (obtained from the set of values $\hat{\mu}_i$) to build fully textured samples keeps all the relevant information for the FM order induced by the structural anisotropy on positions. In other words, the fluctuations of the Ising axes around the mean value \hat{a} play only a marginal role.

For the volume fraction $\Phi = 0.262$ similar results are obtained. Figure 13 exhibits curves of m_1 and χ_m vs T for $\beta_f = 0$ and $\beta_f = 8.5$ [a value larger than $\beta_c(\text{DHS}, \Phi) = 7.7$]. Both

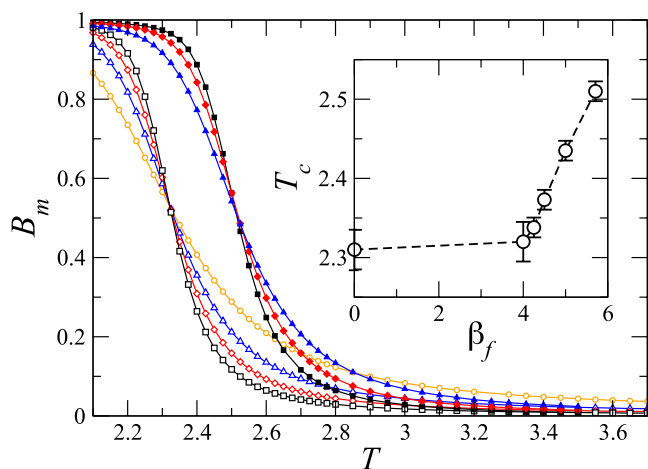


FIG. 12. (a) Plots of B_m vs T for systems of N dipoles placed on anisotropic frozen configurations obtained for $\Phi = 0.45$ and given freezing temperatures β_f . \blacktriangle , \bullet , and \blacksquare stand for $\beta_f = 5.71$ and system sizes $N = 453$, 758 , and 1177 respectively. \circ , \triangle , \diamond , and \square stand for $\beta_f = 0$ and $N = 125$, 216 , 512 , and 1000 , respectively. The solid lines are guides to the eye. The inset shows the PM-FM transition temperature T_c vs β_f for volume fraction $\Phi = 0.45$.

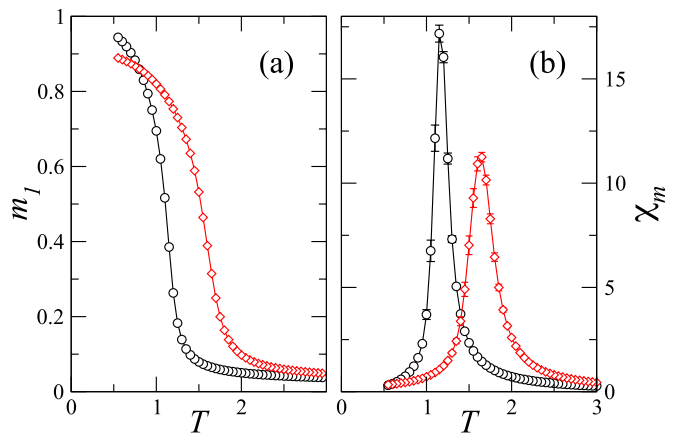


FIG. 13. (a) Plots of the magnetization m_1 vs T for ensembles of $N = 1000$ dipoles placed on anisotropic frozen configurations obtained for $\Phi = 0.262$. Symbols \circ and \diamond stand for $\beta_f = 0$ and 8.5 , respectively. (b) Plots of the susceptibility χ_m vs T for ensembles of $N = 1000$ for $\Phi = 0.262$. Symbols are the same as in (a).

the m_1 and χ_m curves move to the right as β_f is increased, indicating again that the presence of structural anisotropy favors FM order. However, it can be noticed that for very low temperatures the magnetization m_1 for $\beta_f = 8.5$ is lower than for $\beta_f = 0$. This fact can be related to the formation of inhomogeneities in the DHS fluid for low T_f [24,25].

IV. CONCLUSIONS

We studied, using Monte Carlo simulations, the effect of positional disorder on the collective properties of fully textured systems of identical magnetic nanospheres that behave as Ising dipoles along common easy axes.

We first studied frozen isotropic systems of hard spheres obtained along the stable liquid branches with volume fraction Φ ranging from low values up to the freezing point ($\Phi \simeq 0.49$). By analyzing the phase diagram on the T - Φ plane, we found a low-temperature ferromagnetic phase for $\Phi \gtrsim \Phi_o = 0.160(5)$, in good agreement with mean-field calculations that assume complete randomness in positions. This phase exhibits strong long-range order. For $\Phi < \Phi_o$ this ferromagnetic phase disappears, giving rise to a spin-glass phase for temperatures below $T_{sg}(\Phi)$. For strong dilution we found $T_{sg}(\Phi)/\Phi = 1.9(1)$. The nature of the dipolar spin-glass phase is similar to the one observed in other systems of Ising dipoles with strong frozen disorder. Plots of Binder cumulants vs Φ allowed us to obtain the transition line between the ferromagnetic and spin-glass phases. We found neither an appreciable reentrance nor an intermediate region with quasi-long-range ferromagnetic between the FM and SG phases.

We also studied anisotropic spatial systems for $\Phi = 0.45$ and $\Phi = 0.262$. They were obtained by freezing the liquid state of the dipolar hard sphere fluid in its polarized state at sufficiently low temperatures T_f . Such systems develop some texturation as well as anisotropic spatial correlations that increase as T_f is decreased. The ferromagnetic order of parallel dipoles placed on such configurations along their nematic director is enhanced as T_f decreases.

ACKNOWLEDGMENTS

We thank the Centro de Supercomputación y Bioinformática at the University of Málaga, and Institute Carlos I at

the University of Granada for their generous allocations of computer time. J.J.A. also thanks the Italian “Fondo FAI” for financial support and is grateful for the warm hospitality he received during his stay at the Pisa INFN section.

-
- [1] R. P. Cowburn, *Philos. Trans. R. Soc. London, Ser. A* **358**, 281 (2000); R. J. Hicken, **361**, 2827 (2003).
- [2] R. Skomski, *J. Phys.: Condens. Matter* **15**, R841 (2003).
- [3] S. Bedanta and W. Kleeman, *J. Phys. D* **42**, 013001 (2009); S. A. Majetich and M. Sachan, **39**, R407 (2006).
- [4] D. Fiorani and D. Peddis, *J. Phys.: Conf. Ser.* **521**, 012006 (2014).
- [5] E. H. Sánchez, M. Vasilakaki, S. S. Lee, P. S. Normile, M. S. Andersson, R. Mathieu, A. López-Ortega, B. P. Pichon, D. Peddis, C. Binns, P. Nordblad, K. Trohidou, J. Nogués, and J. A. de Toro, *Small* **18**, 2106762 (2022).
- [6] J. A. de Toro, S. S. Lee, D. Salazar, J. L. Cheong, P. S. Normile, P. Muñiz, J. M. Riveiro, M. Hillenkamp, F. Tournus, A. Amion, and P. Nordblad, *Appl. Phys. Lett.* **102**, 183104 (2013); M. S. Andersson, R. Mathieu, S. S. Lee, P. S. Normile, G. Singh, P. Nordblad, and J. A. de Toro, *Nanotechnology* **26**, 475703 (2015); M. S. Andersson, J. A. De Toro, S. S. Lee, P. S. Normile, P. Nordblad, and R. Mathieu, *Phys. Rev. B* **93**, 054407 (2016).
- [7] S. Nakamae, *J. Magn. Magn. Mater.* **355**, 225 (2014).
- [8] J. Luttinger and L. Tisza, *Phys. Rev. B* **72**, 257 (1942); J. F. Fernández and J. J. Alonso, *ibid.* **62**, 53 (2000); J. Batle and O. Ciftja, *Sci. Rep.* **10**, 19113 (2020).
- [9] S. J. Knak Jensen and K. Kjaer, *J. Phys.: Condens. Matter* **1**, 2361 (1989).
- [10] D. Peddis, S. Laureti, and D. Fiorani, *New Trends in Nanoparticle Magnetism*, Springer Series in Materials Science Series Vol. 308 (Springer, Cham, 2021).
- [11] X. Batlle, C. Moya, M. Escoda-Torroella, O. Iglesias, A. Fraile Rodríguez, and A. Labarta, *J. Magn. Magn. Mater.* **543**, 168594 (2022).
- [12] J. Dobson, *Nat. Mater.* **11**, 1006 (2012).
- [13] Q. A. Panhurst, N. T. K. Thanh, S. K. Jones, and J. Dobson, *J. Phys. D* **42**, 224001 (2009); X. Li, J. Wei, K. E. Aifantis, Y. Fan, Q. Feng, F.-Z. Cui, and F. Watari, *J. Biomed. Mater. Res.* **104**, 1285 (2016).
- [14] S. Nakamae, C. Crauste-Thibierge, D. L’Hôte, E. Vincent, E. Dubois, V. Dupuis, and R. Perzynski, *Appl. Phys. Lett.* **101**, 242409 (2012).
- [15] S. Sahoo, O. Petravic, W. Kleemann, P. Nordblad, S. Cardoso, and P. P. Freitas, *Phys. Rev. B* **67**, 214422 (2003).
- [16] S. Mørup, *Europhys. Lett.* **28**, 671 (1994).
- [17] V. Russier and J. J. Alonso, *J. Phys.: Condens. Matter* **32**, 135804 (2020).
- [18] J. J. Alonso, B. Allés, and V. Russier, *Phys. Rev. B* **100**, 134409 (2019).
- [19] V. Russier, J. J. Alonso, I. Lisiecki, A. T. Ngo, C. Salzemann, S. Nakamae, and C. Raepsaet, *Phys. Rev. B* **102**, 174410 (2020).
- [20] J. J. Alonso, B. Allés, and V. Russier, *Phys. Rev. B* **102**, 184423 (2020).
- [21] H. Zhang and M. Widom, *Phys. Rev. B* **51**, 8951 (1995).
- [22] C. Moya, O. Iglesias, X. Batlle, and A. Labarta, *J. Phys. Chem. C* **119**, 24142 (2015).
- [23] J. J. Weis and D. Levesque, *Phys. Rev. E* **48**, 3728 (1993).
- [24] J. J. Weis, *J. Chem. Phys.* **123**, 044503 (2005); C. Holm and J. J. Weis, *Curr. Opin. Colloid Interface Sci.* **10**, 133 (2005).
- [25] J. G. Malherbe, V. Russier, and J. J. Alonso, *J. Phys.: Condens. Matter* **35**, 305802 (2023).
- [26] G. Ayton, M. J. P. Gingras, and G. N. Patey, *Phys. Rev. Lett.* **75**, 2360 (1995); *Phys. Rev. E* **56**, 562 (1997).
- [27] K. M. Tam and M. J. P. Gingras, *Phys. Rev. Lett.* **103**, 087202 (2009); J. J. Alonso and J. F. Fernández, *Phys. Rev. B* **81**, 064408 (2010).
- [28] B. D. Lubachevsky and F. H. Stillinger, *J. Stat. Phys.* **60**, 561 (1990).
- [29] S. Torquato and F. H. Stillinger, *Rev. Mod. Phys.* **82**, 2633 (2010).
- [30] M. Skoge, A. Donev, F. H. Stillinger, and S. Torquato, *Phys. Rev. E* **74**, 041127 (2006).
- [31] E. Marinari and G. Parisi, *Europhys. Lett.* **19**, 451 (1992); K. Hukushima and K. Nemoto, *J. Phys. Soc. Jpn.* **65**, 1604 (1996).
- [32] N. A. Metropolis, A. W. Rosenbluth, M. N. Rosenbluth, A. H. Teller, and E. Teller, *J. Chem. Phys.* **21**, 1087 (1953).
- [33] I. Rozada, M. Aramon, J. Machta, and H. G. Katzgraber, *Phys. Rev. E* **100**, 043311 (2019).
- [34] J. J. Alonso and B. Allés, *J. Phys.: Condens. Matter* **29**, 355802 (2017).
- [35] P. Ewald, *Ann. Phys. (NY)* **369**, 253 (1921).
- [36] Z. Wang and C. Holm, *J. Chem. Phys.* **115**, 6351 (2001).
- [37] M. P. Allen and D. J. Tildesley, *Computer Simulation of Liquids* (Clarendon, Oxford, 1987).
- [38] S. F. Edwards and P. W. Anderson, *J. Phys. F* **5**, 965 (1975).
- [39] M. Palassini and S. Caracciolo, *Phys. Rev. Lett.* **82**, 5128 (1999).
- [40] For some values of Φ , pairs of curves do not cross precisely at the same point, but $1/L$ extrapolations of the crossing points allow us to obtain well-defined values of T_c .
- [41] For volume fractions below $\Phi \approx 0.49$ the HS fluid is in a stable liquid phase. Compressing rapidly, this fluid results in the appearance of metastable branches of amorphous states with densities up to $\Phi \approx 0.64$. For these glassy states with $\Phi \geq 0.49$, the radial distribution function $g(r)$ exhibits characteristic double-horn peaks at $r = \sqrt{3}d$ and $2d$, where d is the diameter or size of the NP. In the absence of local anisotropies, Monte Carlo simulations show that the existence of FM for systems of dipoles in RDP depends on the presence of this double horn.
- [42] M. J. P. Gingras and P. C. W. Holdsworth, *Phys. Rev. Lett.* **74**, 202 (1995).